



## RESEARCH ARTICLE

### PREPARATION OF COST-EFFECTIVE PHOTODEGRADATION CATALYST BASED ON ZINC OXIDE DERIVED FROM ELECTRIC ARC FURNACE DUST AND KAOLINITE

<sup>1</sup>Abdelghaffar S. Dhmees, <sup>1</sup>Raed M. Hegazey, <sup>2,3</sup>Ragaa E. El-Azabawy and <sup>1,\*</sup>Omnia A. A. El-Shamy

<sup>1</sup>Analysis and Evaluation Department, Egyptian Petroleum Research Institute, Nasr City, Cairo 11727, Egypt

<sup>2</sup>Chemistry Department, Faculty of Science, Al-Azhar University (Girls), Nasr City, Cairo, Egypt

<sup>3</sup>Chemistry Department, Faculty of Science and Art –Al Mandaq, Al-Baha University, Kingdom of Saudi Arabia

#### ARTICLE INFO

##### Article History:

Received 28<sup>th</sup> April, 2019

Received in revised form

19<sup>th</sup> May, 2019

Accepted 07<sup>th</sup> June, 2019

Published online 31<sup>st</sup> July, 2019

##### Key Words:

Electric arc Furnace Dust, Zinc Oxide,  
Photo-Catalysis, Water Treatment.

##### \*Corresponding author:

Omnia A. A. El-Shamy

Copyright © 2019, Abdelghaffar S. Dhmees, Raed M. Hegazey, Ragaa E. El-Azabawy and Omnia A. A. El-Shamy. This is an open access article distributed under the Creative Commons Attribution License, which permits unrestricted use, distribution, and reproduction in any medium, provided the original work is properly cited.

Citation: Abdelghaffar S. Dhmees, Raed M. Hegazey, Ragaa E. El-Azabawy and Omnia A. A. El-Shamy. 2019. "Preparation of cost-effective photodegradation catalyst based on zinc oxide derived from electric arc furnace dust and kaolinite.", *International Journal of Current Research*, 11, (07), 5840-5846.

#### ABSTRACT

The disposal of industrial waste in a secure manner is the concern of many countries in the world. Herein, zinc oxide obtained from dangerous waste "Electric Arc Furnace Dust (EAFD)" that produced from steel manufacture. In addition, raw Egyptian kaolinite (white kaolinite and rich iron kaolinite) are used to enhance the photocatalytic activity of the separated ZnO by the formation of W-K@ZnO and Fe-K@ZnO, respectively. X-ray diffraction spectroscopy, BET surface area, and photoluminescence measurements are utilized to estimate the chemical structure of the prepared materials. The results show that the combination of rich iron kaolinite with ZnO enhance the photodegradation up to 98.2%. The presence of Fe<sub>2</sub>O<sub>3</sub> promotes the absorption of ZnO into the visible region and delay the electron-hole recombination.

## INTRODUCTION

Electric Arc Furnace Dust (EAFD) is generally produced from steelmaking with high amount. Also, the overall increment production of steel leads to dispose of the high amount of EAFD as waste, where 20 kg of EAFD is produced from every ton of steel iron. The world generation of EAFD is assessed to be 5–7 million tons for every year (Oustadakis *et al.*, 2010). Along these lines, the EAFD are considered as dangerous waste. The recycling of wasted EAFD is worthy not only to human health and ecological integrity, yet in an economic viewpoint to resources and materials. The fundamental contents of EAFD are iron (24.0–45.5%) and zinc (8.0–33.0%), in addition to a traces amount of harmful elements, such as Cu (0.2–0.4%), Cd (<0.12%), Ni (<0.1%), Mn (1.68–4.2%), Cr (<0.5%), Si (0.35–2.5%), Pb (0.2–5.6%) and Ca (0.9–3.4%) (Xanthopoulos *et al.*, 2017). Also, Fe<sub>3</sub>O<sub>4</sub>, MgFe<sub>2</sub>O<sub>4</sub>, ZnFe<sub>2</sub>O<sub>4</sub>, FeCr<sub>2</sub>O<sub>4</sub>, SiO<sub>2</sub>, Ca<sub>0.15</sub>Fe<sub>2.85</sub>O<sub>4</sub>, Mn<sub>3</sub>O<sub>4</sub>, MgO, and ZnO phases are present as traces in EAFD (Machado *et al.*, 2006). Zinc is considered as the most significant component in the EAFD because of its moderately substantial sum and wide application (Dutra *et al.*, 2006). In this manner, the particular recuperation of zinc from EAFD with a high rate is an appealing alternative considering its low production cost. To date, numerous procedures have been or are being examined worldwide to recoup zinc from the EAFD

(Xia and Picklesi 2000; Havlik *et al.*, 2005; Ruiz *et al.*, 2007; Oustadakis *et al.*, 2010; Shawabkeh 2010). So, metallurgical methods can be applied by pyro-metallurgical like carbothermic reduction which required high energy consumption. However, just 70% of all-out zinc can be recovered. In view of these defies, hydrometallurgical methods with different variation like high-pressure acid leaching, (Zhang *et al.*, 2011) microwave alkaline leaching and two-stage leaching of acid (Herrero *et al.*, 2010) or concentrated caustic solutions have been investigated (Zhang *et al.*, 2011). The previous data declared that the hydrometallurgical method has an efficiency, in the case of Zinc, ranged from 73% to 100% (de Souza *et al.*, 2001; Li and Xi 2005). ZnO has a wurtzite hexagonal structure and it is classified as n-type semiconductor that possesses large band gap "3.3 eV". Also, it has a high refractive index value (> 2) which alongside the extensive exciton binding energy (BE) of 60 meV, makes this material appropriate for various optoelectronic applications (Gallegos *et al.*, 2018). Among various semiconductors utilized as photo-catalysts, TiO<sub>2</sub> is the most studied oxide. In any case, ZnO is used as an alternative of TiO<sub>2</sub> because of its comparable band gap Energy, low effective cost. Additionally; the photoactivity of ZnO in some cases become better than that of TiO<sub>2</sub> (Soltani *et al.*, 2014). This study aimed to prepare zinc oxide via eco-friendly and facile method using Zinc ions solution that obtained from EAFD. Besides, the prepared ZnO

is incorporated with two different raw Egyptian Kaolinite: white Kaolinite, and Kaolinite rich iron, to obtain W-K@ZnO and Fe-K@ZnO, respectively. The crystal structures of the composites are obtained using XRD. Also, EDX and specific surface area measurements are investigated for the prepared materials. The photocatalytic efficiency of W-K@ZnO and Fe-K@ZnO for reactive yellow 145 dye (Ry145) investigated under visible light. Additionally, Photo Luminesces spectra used to study the performance of charge trapping and to detect the destination of photo generated electrons - holes "e-h" in the prepared materials.

## EXPERIMENTAL

### Materials

Analytical-reagent (AR) grade HCl (37%), NaOH, and H<sub>2</sub>O<sub>2</sub> purchased from Aldrich, Germany. Electric Arc Furnace Dust (EAFD) used in this work supplied by El-EZZ company for steel (Suez, Egypt). Reactive yellow 145 (Ry145) obtained from Merck, Germany.

**Separation of Zinc from the EAFD:** Scheme 1 Declares the separation of zinc ions from EAFD. Firstly, 40 g of EAFD powder (>160µm) was mixed with a 400 mL of 2M H<sub>2</sub>SO<sub>4</sub> at 90 °C for 3 h. After being adequately leaching, the solution was transferred through filter paper (42) to separate the residue of Silica, CaSO<sub>4</sub>, and PbSO<sub>4</sub>. Firstly, transfer the leaching solution (containing Zn<sup>2+</sup>, Fe<sup>3+</sup>, etc.) to 500 mL volumetric flask and complete using deionized (DI) water. Then, the obtained residue is washed three times using DI water and put in an oven at 100°C (24 h). To precipitate ferric ions as a Fe(OH)<sub>3</sub>, the pH of leaching solution is adjusted using 1M NaOH (pH 5.2) then collect the precipitate. To obtain zinc hydroxide; the supernatant of the previous solution (after separation of Fe(OH)<sub>3</sub>) is adjusted at a pH of 8.0, then Zn(OH)<sub>2</sub> precipitated. The precipitated ZnO was washed and dried (105°C) for 24 h (Wang *et al.*, 2016; Xing *et al.*, 2017).

**Characterizations methods:** The crystal structure of the prepared ZnO was confirmed using X-ray diffraction (XRD) using ANalytical XPERT PRO MPD, Netherland. The angle range (2θ = 4-80°) scanned using a nickel-filtered Cu Kα radiation source with wave length of 0.154 nm). The surface area of the synthesized samples is determined from nitrogen isotherms (196 °C) on Quantachrome analyzer (Nova 2000 series). Energy dispersive x-ray spectroscopic (EDX) technique is used to detect the components of the clay. Photoluminescence (PL) analysis of the samples examined using Perkin Elmer-LS-55 fluorescence spectrophotometer (λ<sub>ex</sub> = 325 nm) at 25 °C.

**Photocatalytic degradation:** Reactive yellow 145 dye (Ry145) was used as a model pollutant to study the performance of W-K@ZnO and Fe-K@ZnO as photo-catalysts under visible light. 15 mg of each photo-catalyst added to 50 ml of the Ry145 aqueous solution (C<sub>0</sub>=30 mg/L). Firstly, the solution mixture stirred in absence of light for half an hour to reach the adsorption-desorption equilibrium. At that point, 500 W linear halogen lamp (λ =420-600nm) as a visible source at 25 °C is used with a constant distance of 15 cm between the dye solution and light source. Each 20 min, 2.5 ml of the sample solution withdrawn and centrifuged to remove the photo-catalyst. UV/VIS spectrophotometer used to detect the concentrations during the experiment.

The Photocatalytic efficiency percentage of degradation for W-K@ZnO and Fe-K@ZnO were calculated using the next equation,

$$\text{Photocatalytic degradation \%} = (C_0 - C) / C_0 \times 100 \quad (1)$$

Where, C<sub>0</sub> is the initial concentration of Ry145, C is the final concentration after degradation.

## RESULTS AND DISCUSSION

The XRD pattern of (W-Kaolinite&W-K@ZnO) and (Fe-Kaolinite &Fe-K@ZnO) are present in Fig. 1 (a and b), respectively. Fig. 1(a) shows diffraction peaks at 2θ of 11.85, 24.38 and 37.19 for W-Kaolinite which corresponding to the (001), (002) and (003) crystallographic plane of Al<sub>2</sub>Si<sub>2</sub>O<sub>5</sub>(OH)<sub>4</sub> which considered as the main chemical composition of Kaolinite. Moreover, the peaks corresponding to SiO<sub>2</sub> and Fe<sub>2</sub>O<sub>3</sub> are detected. Also, peaks at 31.93°, 34.57°, 36.41°, 47.75°, 56.83°, 62.87°, 68.35°, 72.55° and 77.21°, attributed to 100, 002, 101, 102, 110, 103, 112, 004 and 202 crystal planes of ZnO, respectively, which reveals that ZnO in W-K@ZnO has hexagonal wurtzite structure (El-Fawal and El-Shamy 2019). Similar characteristic peaks for Kaolinite and ZnO are present in Fig. 1(b) for Fe-Kaolinite and Fe-K@ZnO, respectively. All the X-ray peaks are matched well with those of the correspondence compounds listed in JCPDS file No. 19-0629. Fig. 2 and 3 display the main compositions of W-Kaolinite and Fe-Kaolinite. Also, Fig. 4 and 5 manifest the presence of ZnO in W-K@ZnO and Fe-K@ZnO, respectively. It is clear that the percentage of Fe in Fe-Kaolinite sample is grater than that of W-Kaolinite.

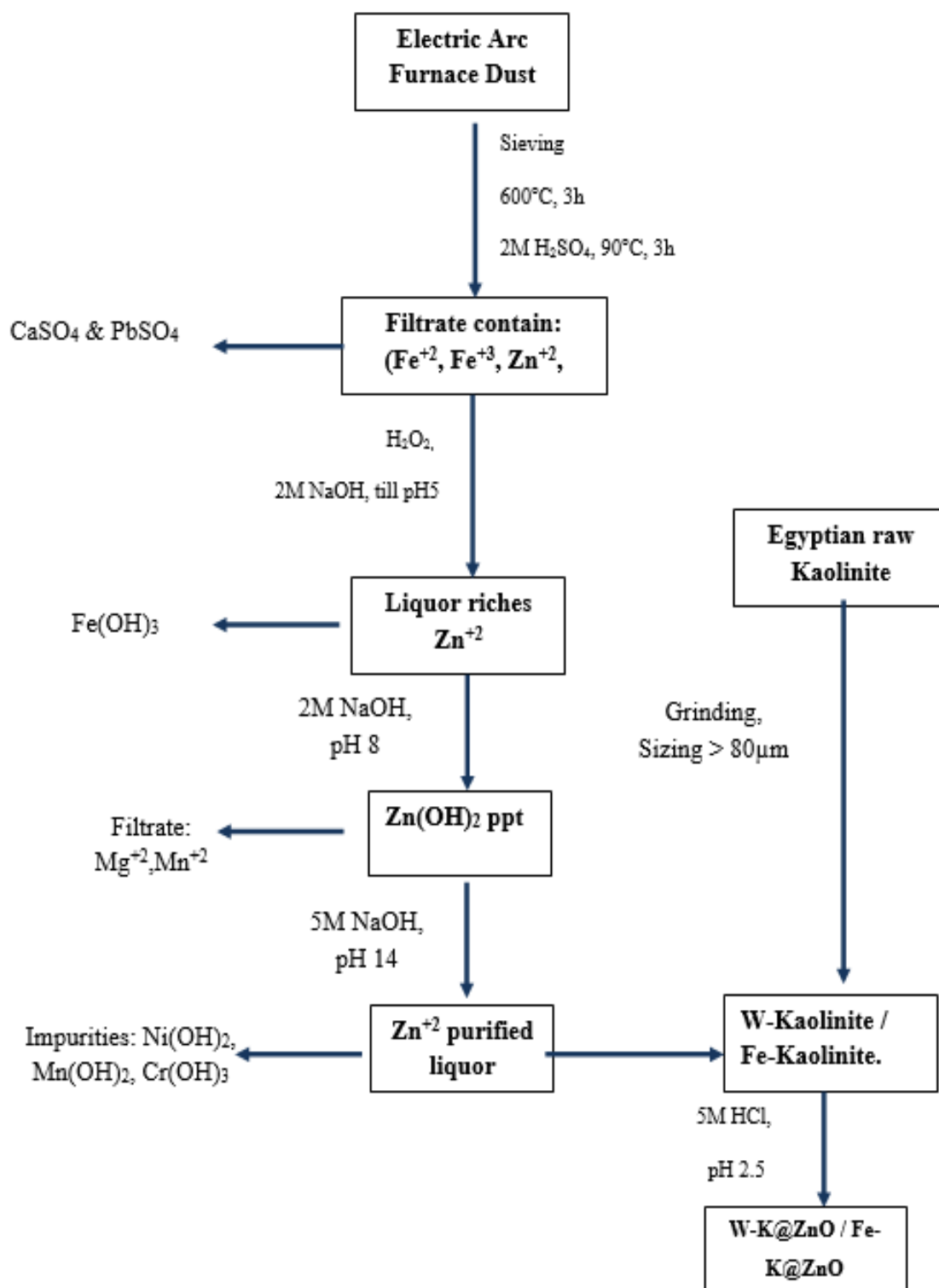
Barrett-Emmett-Teller method is used to determine the surface properties and pore surface parameters for the prepared materials. Fig. 6 shows type IV isotherm for both W-Kaolinite and Fe-Kaolinite with relative hysteresis loops of type H3, indicating mesoporous structure (Kruk and Jaroniec 2001). The surface area of Fe-K@ZnO (44.148 m<sup>2</sup>/g) is greater than W-K@ZnO (16.808 m<sup>2</sup>/g), pointing out more surface active site for adsorption. Fig.7 represent a narrow pore size distribution of W-K@ZnO and Fe-K@ZnO derived from the desorption branch of the N<sub>2</sub> adsorption/desorption isotherm. ZnO@Fe-Kaolinite has larger pore volume than W-K@ZnO which give more adsorption efficiency of contaminant in the aqueous system. The surface area, pore volume and the average pore size of W-K@ZnO and Fe-K@ZnO are listed in Table 1. The optical properties of W-K@ZnO and Fe-K@ZnO are detected via Photoluminescence measurements. Since, zinc oxide is highly efficient as photo-catalyst. The combination of ZnO with Kaolinite should affect its photocatalytic properties. Fig.8 shows two emission peaks of 393 nm and 447 nm assigned to the near band edge emission that results from the recombination of free excited e-h formed when excited by radiation of energy greater or equal to the energy of the band gap and the deep level emission that results from several intrinsic defects like zinc interstitials, zinc vacancies, interstitial oxygen and oxygen vacancies (Ding *et al.*, 2012; Karunakaran *et al.*, 2012; Hosseini *et al.*, 2015). The presence of oxygen in Kaolinite increase the intensity of these peaks. Concerning on Fig.8, the blue emission peak around 465 nm that continuous to the green region (≈ 560 nm) attributed to the presence of ZnO and this coincides with results in the literature (Yogamalar *et al.*, 2011; El-Fawal and El-Shamy 2019). The presence of iron in Fe-K@ZnO results in a red shift emission.

**Table 1. The surface properties and pore structure Parameters for W-K@ ZnO and Fe-K@ ZnO.**

	Surface area (m <sup>2</sup> /g)	Pore volume, (cm <sup>3</sup> /g)	Pore diameter, (nm)
W-K@ ZnO	16.808	0.044	3.485
Fe-K@ ZnO	44.148	0.097	3.681

**Table 2. Kinetic Parameters for and degradation Efficacy of W-K@ZnO and Fe-K@ZnO**

	K <sub>a</sub> (min <sup>-1</sup> )	R <sup>2</sup>	Degradation (%)
W-K@ZnO	0.0147	0.9967	94.5 %
Fe-K@ZnO	0.0219	0.9909	98.2 %

**Scheme 1. Extraction of Zinc oxide and formation of W-K@ZnO and Fe-K@ZnO**

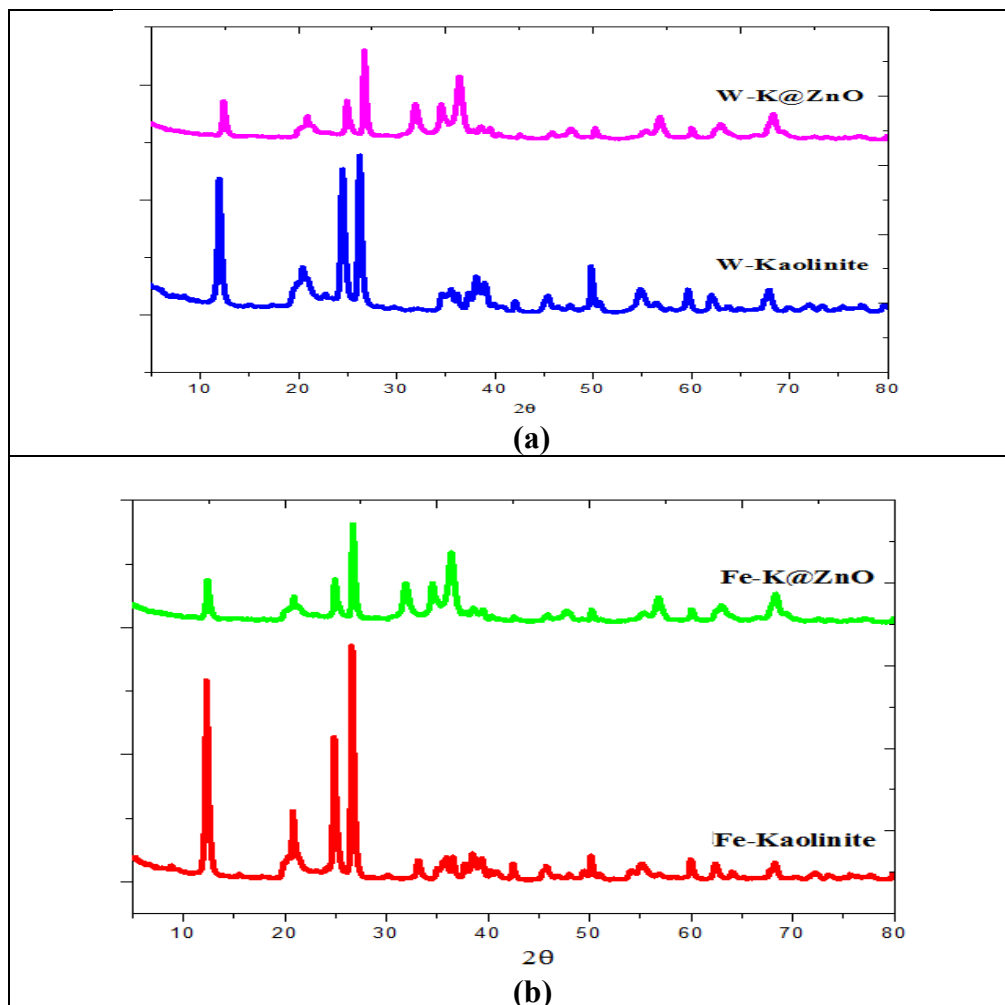


Fig. 1. XRD of (a) W-Kaolinite, W-K@ZnO, and (b) Fe-Kaolinite, Fe-K@ZnO

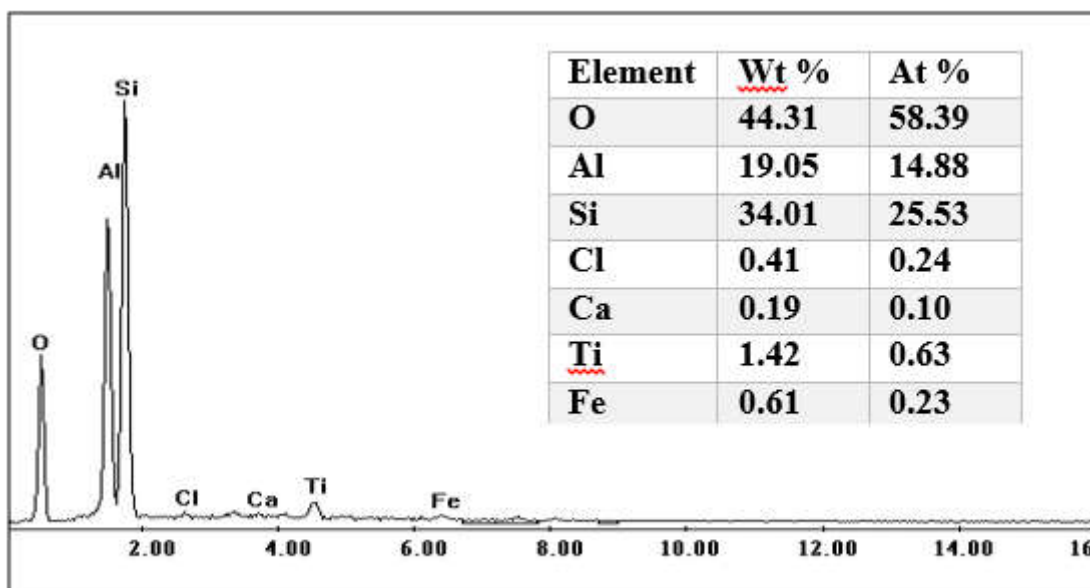


Fig. 2. The EDX of W-Kaolinite

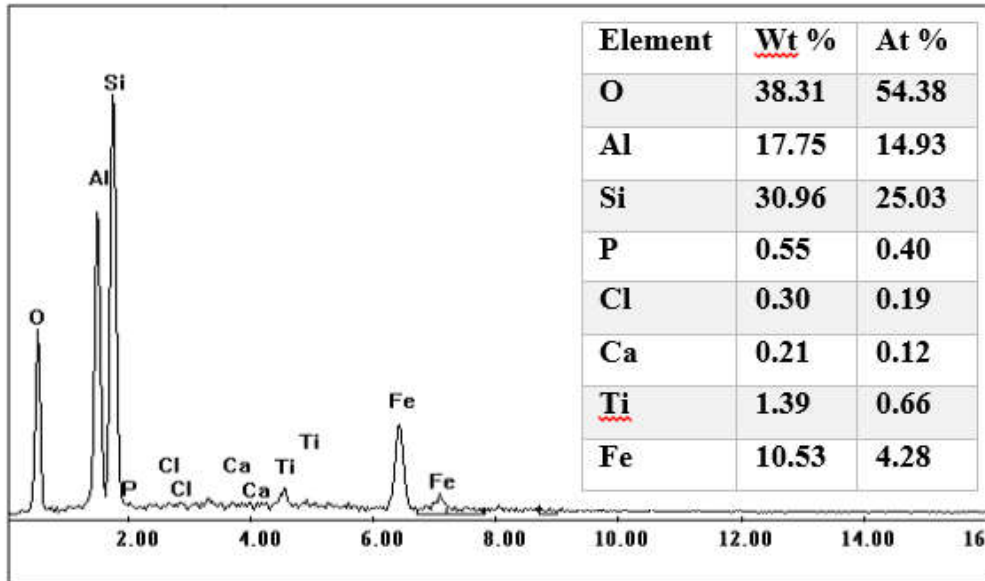


Fig. 3: The EDX of Fe-Kaolinite

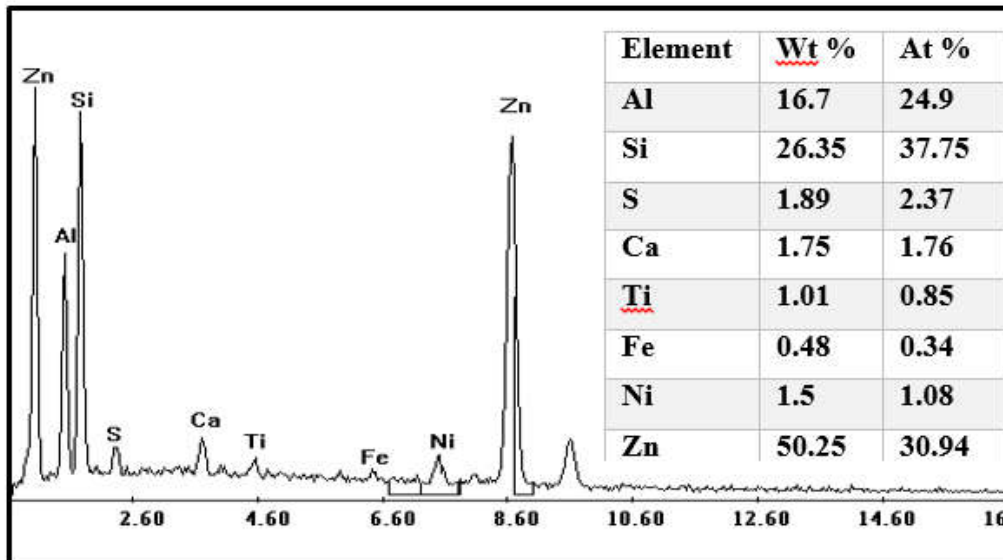


Fig. 4. The EDX of W-K@ZnO

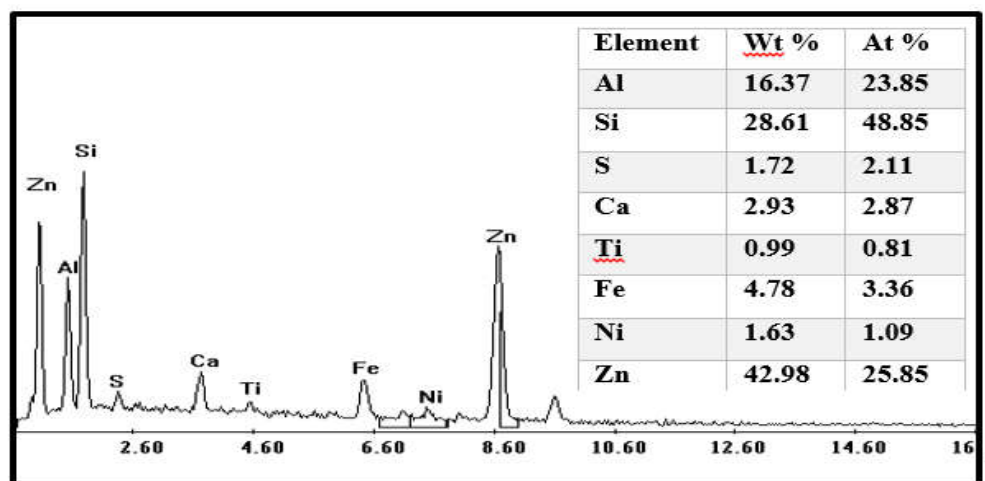


Fig. 5. The EDX of Fe-K@ZnO

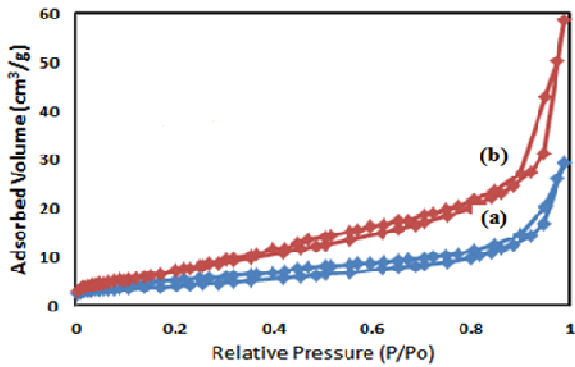


Fig. 6. Isotherm hysteresis loop of (a) W-K@ZnO and (b) Fe-K@ZnO

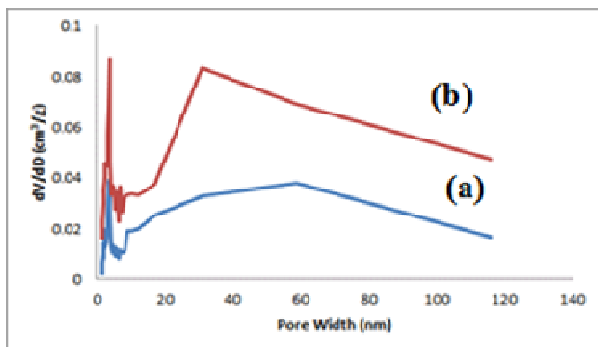


Fig. 7. Pore size distribution of (a) W-K@ZnO and (b) Fe-K@ZnO

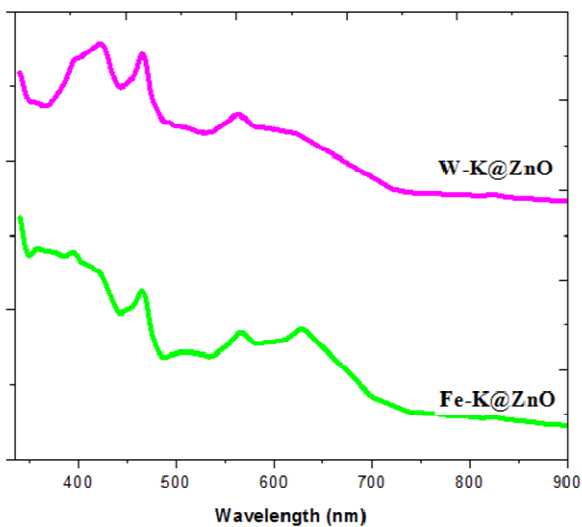


Fig. 8. Photoluminescence spectra of W-K@ZnO and Fe-K@ZnO

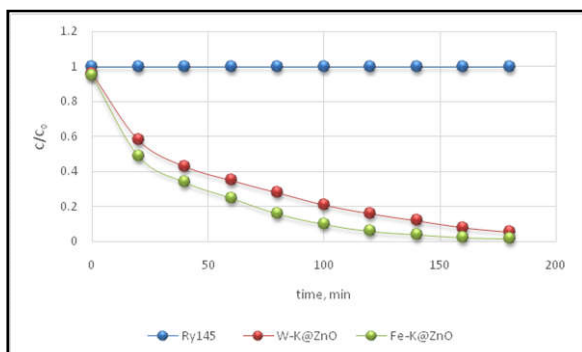


Fig. 9. Photodegradation of Ry145 by W-K@ZnO and Fe-K@ZnO

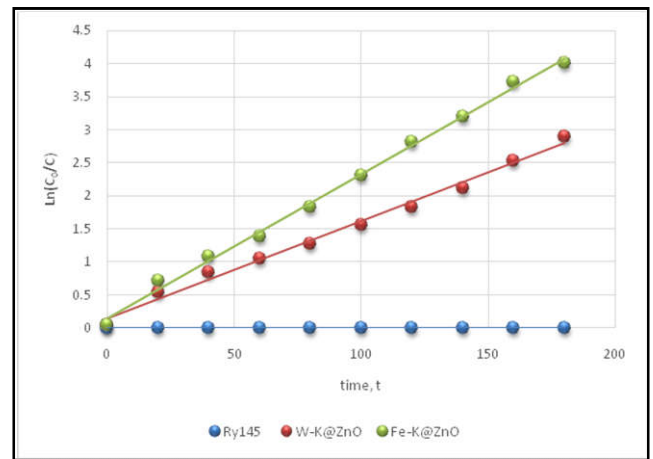


Fig. 10. Kinetics of Ry145 degradation by W-K@ZnO and Fe-K@ZnO

peak of 630nm, indicating an additional energy level in the band gap. Moreover, Fig.8 shows a quenching of PL intensity for Fe-K@ZnO comparing by W-K@ZnO indicating that the recombination of the photogenerated charge carriers was reduced in the presence of higher percentage of iron.

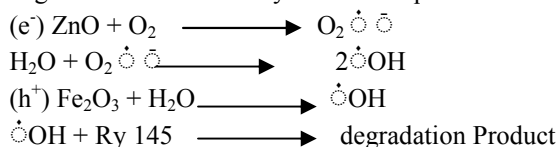
**Photocatalytic study:** The photocatalytic performance of W-K@ZnO and Fe-K@ZnO assessed for the degradation of Ry145 under visible light. The Ry145 is hard to photodegrade without a photo-catalyst. The adsorption-desorption equilibrium set up after half an hour in dark. Fig. 9 shows the degradation percentage of Ry145, which has values of 94.5 % and 98.2 % for W-K@ZnO and Fe-K@ZnO, respectively. It is notable that the improvement of the photocatalytic action for any photocatalytic substance relies upon the separation efficacy of the electron-hole pairs "e-h", the surface area and the ability of absorption for light (Liu *et al.*, 2016). Subsequently, the great efficacy for Fe-K@ZnO as a photo-catalyst is straightforwardly identified with its high surface area compared with W-K@ZnO. In addition, the quenching of its photoluminescence (Fig. 8) due to the existence of Fe<sub>2</sub>O<sub>3</sub>. The rate of photodegradation reaction was represented by linear kinetic curves as shown in Fig. 10. The photocatalytic process obeys a Langmuir first-order kinetics model which obtained from the next equation:

$$\ln C_0/C = K_a t \quad (2)$$

Where:  $C_0$  is the initial concentration,  $C$  is the concentration of Ry145 at time  $t$  and  $K_a$  is the apparent first-order rate constant. The data listed in Table 1 represented that Fe-K@ZnO exhibits higher rate constant ( $0.0219 \text{ min}^{-1}$ ). This result coincided with the data obtained from photoluminescence and surface area measurements. Concerning the previous data, it is apparent that Fe-K@ZnO demonstrate a high surface area and great properties for the separation of photo-induced e-h pairs of ZnO. These emphasize cause increment in the photocatalytic performance under visible light, as demonstrated by their better efficacy in the degradation of Ry145 under visible light (Table 2) (El-Fawal and El-Shamy 2019).

**Photodegradation mechanism:** The degradation mechanism of Ry145 by Fe-K@ZnO discussed based on that ZnO is an n-type semiconductor, while Fe<sub>2</sub>O<sub>3</sub> is a p-type one. So, the band gap of Fe<sub>2</sub>O<sub>3</sub> is lower than those of ZnO and vice versa. When they are in contact, Fe<sub>2</sub>O<sub>3</sub> can expand the lifetime of charge

carriers. Also, the Fermi level of ZnO is downward and that of Fe<sub>2</sub>O<sub>3</sub> is upward until a balance is settled. Under light exposure, electrons and holes are generated in the junction. The photogenerated electrons in the conduction band of Fe<sub>2</sub>O<sub>3</sub> cannot transfer to that of n-type "ZnO" due to the barrier formed at the Junction. Moreover, the photo generated holes in ZnO emigrate from the valence band of ZnO to that of p-type "Fe<sub>2</sub>O<sub>3</sub>" because of the gradient established at the junction. Thus, the overabundant negative charge in the ZnO. The photo degradation reaction obeys the next equation:



## Conclusion

Zinc oxide was obtained with low cost from industrial waste (Electric Arc Furnace Dust). Then, photocatalytic compounds, W-K@ZnO, and Fe-K@ZnO obtain from mixing White Kaolinite (W-K) and iron rich kaolinite (Fe-K) with the prepared ZnO, respectively. The prepared composites are confirmed by XRD and EDX measurements. Fe-K@ZnO has higher photocatalytic activity (98.2%) comparing by W-K@ZnO for photodegradation of Ry 145 under visible light due to its lower PL intensity and higher surface area. Moreover, the presence of Fe<sub>2</sub>O<sub>3</sub> enhances its photocatalytic behavior by increase the electron-hole separation for ZnO. Also, Fe<sub>2</sub>O<sub>3</sub> caused additional energy level that presents in Photoluminescence analysis (red shift emission). From this work, it is spotted that Fe-K@ZnO is an excellent photocatalyst with a low cost for the photodegradation of Ry 145 as an organic pollutant.

## REFERENCES

De Souza CCBM., de Oliveira DC., Tenório JAS. 2001. Characterization of used alkaline batteries powder and analysis of zinc recovery by acid leaching. *Journal of Power Sources* 103:120–126

Ding J., Yan X., Xue Q. 2012. Study on field emission and photoluminescence properties of ZnO/graphene hybrids grown on Si substrates. *Materials Chemistry and Physics* 133:405–409

Dutra AJB., Paiva PRP., Tavares LM. 2006. Alkaline leaching of zinc from electric arc furnace steel dust. *Minerals engineering* 19:478–485

El-Fawal EM., El-Shamy OAA. 2019. Photodegradation enhancement of 2-chlorophenol using ZnO–CdS@CS nanocomposite under visible light. *International Journal of Environmental Science and Technology*. doi: 10.1007/s13762-019-02249-y

Gallegos M V., Aparicio F., Peluso MA. *et al.*, 2018. Structural, optical and photocatalytic properties of zinc oxides obtained from spent alkaline batteries. *Materials Research Bulletin* 103:158–165

Havlik T., Turzakova M., Stopic S., Friedrich B. 2005. Atmospheric leaching of EAF dust with diluted sulphuric acid. *Hydrometallurgy* 77:41–50

Herrero D., Arias PL., Güemez B. *et al* 2010. Hydrometallurgical process development for the production of a zinc sulphate liquor suitable for electrowinning. *Minerals engineering* 23:511–517

Hosseini SM., Sarsari IA., Kameli P., Salamati H. 2015 Effect of Ag doping on structural, optical, and photocatalytic properties of ZnO nanoparticles. *Journal of Alloys and Compounds* 640:408–415

Karunakaran C., Jayabharathi J., Jayamoorthy K., Vinayagamorthy P. 2012. Inhibition of fluorescence enhancement of benzimidazole derivative on doping ZnO with Cu and Ag. *Journal of Photochemistry and Photobiology A: Chemistry* 247:16–23

Kruk M., Jaroniec M. 2001. Gas adsorption characterization of ordered organic–inorganic nanocomposite materials. *Chemistry of materials* 13:3169–3183

Li Y., Xi G. 2005. The dissolution mechanism of cathodic active materials of spent Zn–Mn batteries in HCl. *Journal of hazardous materials* 127:244–248

Liu H., Hao H., Xing J. *et al.*, 2016. Enhanced photocatalytic capability of zinc ferrite nanotube arrays decorated with gold nanoparticles for visible light-driven photodegradation of rhodamine B. *Journal of materials science* 51:5872–5879

Machado JGMS., Brehm FA., Moraes CAM., *et al.*, 2006. Chemical, physical, structural and morphological characterization of the electric arc furnace dust. *Journal of hazardous materials* 136:953–960

Oustadakis P., Tsakiridis PE., Katsiapi A., Agatzini-Leonardou S. 2010. Hydrometallurgical process for zinc recovery from electric arc furnace dust (EAFD): Part I: Characterization and leaching by diluted sulphuric acid. *Journal of hazardous materials* 179:1–7

Ruiz O., Clemente C., Alonso M., Alguacil FJ. 2007. Recycling of an electric arc furnace flue dust to obtain high grade ZnO. *Journal of hazardous materials* 141:33–36

Shawabkeh RA. 2010. Hydrometallurgical extraction of zinc from Jordanian electric arc furnace dust. *Hydrometallurgy* 104:61–65

Soltani RDC., Rezaee A., Khataee AR., Safari M. 2014. Photocatalytic process by immobilized carbon black/ZnO nanocomposite for dye removal from aqueous medium: Optimization by response surface methodology. *Journal of Industrial and Engineering Chemistry* 20:1861–1868

Wang H., Li Y., Gao J., *et al.*, 2016. A novel hydrothermal method for zinc extraction and separation from zinc ferrite and electric arc furnace dust. *International Journal of Minerals, Metallurgy, and Materials* 23:146–155

Xanthopoulos P., Agatzini-Leonardou S., Oustadakis P., Tsakiridis PE. 2017. Zinc recovery from purified electric arc furnace dust leach liquors by chemical precipitation. *Journal of environmental chemical engineering* 5:3550–3559

Xia DK., Pickles CA. 2000. Microwave caustic leaching of electric arc furnace dust. *Minerals Engineering* 13:79–94

Xing P., Ma B., Zeng P. *et al.*, 2017. Deep cleaning of a metallurgical zinc leaching residue and recovery of valuable metals. *International Journal of Minerals, Metallurgy, and Materials* 24:1217–1227

Yogamalar NR., Ashok M., Bose AC. 2011. Blue emission and bandgap modification in N: ZnO nanorods. *Functional Materials Letters* 4:271–275

Zhang Y., Yu X., Li X. 2011. Zinc recovery from franklinite by sulphation roasting. *Hydrometallurgy* 109:211–214